Global shape of the magnetotail current sheet as derived from Geotail and Polar data

N. A. Tsyganenko

Universities Space Research Association and Laboratory for Extraterrestrial Physics, NASA Goddard Space Flight Center, Greenbelt, Maryland, USA

D. H. Fairfield

Laboratory for Extraterrestrial Physics, NASA Goddard Space Flight Center, Greenbelt, Maryland, USA

Received 27 May 2003; revised 13 November 2003; accepted 29 January 2004; published 24 March 2004.

[1] An analytical approximation is developed for the shape of the nightside tail current sheet, representing it as a function of the Earth's dipole tilt angle, solar wind ram pressure, and the interplanetary magnetic field (IMF). The model is based on 5-min average magnetometer data of the Geotail and Polar spacecraft, spanning the periods 1994–2002, and 1999–2001, respectively. All the magnetospheric data were tagged by concurrent values of the solar wind dynamic pressure and IMF B_y and B_z components, averaged over 30-min intervals immediately preceding the magnetospheric observations. Warping and twisting parameters were calculated by minimizing the number of mismatches between the observed and predicted orientation of the magnetic field on both sides of the model current sheet. The model is valid within the nightside magnetosphere in the range of tailward distances $-50\ R_E \leq X_{GSM} \leq 0$. Variations of the solar wind pressure P change the shape of the deformed current sheet in such a way that an increase of P results in a decrease of the magnetotail "hinging distance" R_H, but increases the magnitude of its transverse warping. The IMF B_z component affects the magnitude of the seasonal/diurnal motion of the current sheet in the north-south direction, and it also controls the degree of the IMF B_y-related twisting, which becomes much larger during the periods with northward IMF B_z. *INDEX TERMS:* 2740 Magnetospheric Physics: Magnetospheric configuration and dynamics; 2708 Magnetospheric Physics: Current systems (2409); 2744 Magnetospheric Physics: Magnetotail; 2753 Magnetospheric Physics: Numerical modeling; 2784 Magnetospheric Physics: Solar wind/magnetosphere interactions

Citation: Tsyganenko, N. A., and D. H. Fairfield (2004), Global shape of the magnetotail current sheet as derived from Geotail and Polar data, *J. Geophys. Res.*, *109*, A03218, doi:10.1029/2003JA010062.

1. Introduction

[2] The tail current sheet is a major source of the external magnetospheric field, and one of principal boundaries in the magnetosphere, defining its global geometry. Predicting the position of the tail current is important for the planning the science of magnetospheric missions and accurately interpreting their results. It is also crucial for the development of empirical models of the magnetospheric fields and plasmas.

[3] The shape of the tail current sheet as a function of the dipole tilt and interplanetary conditions was addressed in numerous studies, using both magnetometer data [e.g., *Russell and Brody*, 1967; *Fairfield*, 1980; *Gosling et al.*, 1986; *Dandouras*, 1988; *Lopez*, 1990; *Nakai et al.*, 1997; *Tsyganenko et al.*, 1998] and the plasma sheet particle data [*Owen et al.*, 1995]. These studies, based on different data sets and techniques, established main features of the current sheet geometry and quantified its location using various analytical approximations. The fundamental effect of the seasonal and diurnal oscillation of the dipole tilt angle is a periodic warping of the neutral sheet surface, so that it bends northward (or southward) near the midnight meridian, but moves in the opposite direction or stays at rest near the tail's flanks. The IMF B_y component was predicted [*Russell*, 1972] and found [*Sibeck et al.*, 1985] to exert a torque on the Earth's magnetotail, resulting in a left- or right-handed twisting of the cross-tail current sheet for positive or negative B_y, respectively.

[4] A common shortcoming of all previous efforts is that they are limited to relatively narrow intervals of distance and they do not provide a global quantitative approximation of the deformed current sheet. Another limitation is the largely incomplete information on the effects of the variable interplanetary conditions, partially due to a limited coverage of the early magnetospheric observations by concurrent solar wind and IMF data. An effort to fill that gap was made by *Owen et al.* [1995], who analyzed the effects of the IMF B_y and B_z on the orientation of the plasma sheet using energetic ion data of ISEE-3, as well as by *Maezawa et al.*

[1997] and *Maezawa and Hori* [1998], who used deep-tail plasma and magnetic field data of Geotail. However, their results were limited to the middle and distant tail, and no attempt was made to empirically represent the shape of the neutral sheet.

[5] In our recent work [*Tsyganenko et al.*, 1998], the warping and twisting effects were quantitatively studied using a set of Geotail magnetometer data taken inside the magnetotail in the interval $-100 < X < -10\ R_E$. The data were binned into 7 intervals of X, and the shape of the warped/twisted current sheet was found separately for each bin by fitting a simple "local" tail field model to the data. It was shown that the amplitude of the tilt-related motion of the midnight part of the current sheet did not decrease with tailward distance and remained at a nearly constant level up to $X \sim -100\ R_E$. In contrast, the transverse warping was found to gradually fade away with the distance.

[6] However, in that work we did not try to develop a unified empirical model that would analytically describe the deformation as a function of X. Neither was any attempt made to include effects of the solar wind ram pressure or those of the IMF B_z. In addition, we used a fitting criterion based on an oversimplified (Harris-type) tail field variation across the current sheet. As was shown in a later study [*Tsyganenko*, 1998], the warping in the YZ plane is accompanied by a north-south asymmetry of the lobe field magnitude, especially pronounced in the near-Earth tail. That effect could result in biased values of the warping parameters. Finally, much new data has become available, owing to the extended near-tail phase of the Geotail mission and due to the gradual shift of the apogee of Polar to low latitudes, which made it possible to densely sample the inner magnetosphere inside $R = 9\ R_E$, relatively poorly explored by previous missions.

[7] The present work is intended to fill in the gaps left in earlier studies. Based on a new set of Geotail and Polar data, we derive here a model representing the shape of the tail neutral sheet on the nightside as a function of position along and across the tail, dipole tilt angle, solar wind ram pressure, and IMF B_y and B_z.

2. Data

[8] Compared with previous studies of this kind, this work uses the largest set of observations, made in the low-latitude magnetosphere and covering the range of distances from 3 to 50 R_E. It comprises magnetometer and plasma instrument data of Geotail taken between January 1994 and July 2002, and magnetometer data of Polar for the period from January 1999 to March 2002. All magnetospheric data records (5-min averages) have been tagged with concurrent values of the solar wind and IMF parameters, as detailed below.

2.1. Interplanetary Medium Data

[9] As in our previous study based on Geotail observations [*Tsyganenko et al.*, 1998], the concurrent solar wind and IMF data are crucial not only for parameterizing the model, but also in the initial selection of the magnetospheric data. The interplanetary data came from ACE (1998–2002), WIND (1994–2002), and IMP 8 (1994–2000) observations. The original high-resolution data were initially averaged over 5-min intervals and extrapolated in space and time from spacecraft locations to Earth by using observed components of the solar wind velocity. From 1998 on, when both ACE and Wind data became available, we usually preferred Wind data, especially when the spacecraft was located closer to Earth than ACE. However, the percentage of Wind data used dropped significantly for the last few years, because the orbital maneuvers made after 1999 often placed the spacecraft apogee far away from the Sun-Earth line. In this regard, we note that all data taken on solar wind streamlines passing farther than $\rho = 40\ R_E$ from the Earth center were discarded, based on the observed deterioration of correlations in the solar wind data with growing ρ [e.g., *Richardson and Paularena*, 2001, and references therein]. More details on the solar wind data preparation can be found in our earlier publications [*Tsyganenko et al.*, 1999; *Tsyganenko*, 2002b].

[10] Because of the well-known windsock effect, data-based studies of the magnetotail structure require an accurate information on the direction of the solar wind flow. As detailed below, before deriving the shape of the neutral sheet from the data, we converted the observed magnetospheric magnetic field vectors into the GSW coordinate system, whose X-axis is antiparallel to the actual direction of the solar wind at the observation time. In this regard, it is interesting to assess the extent of the typical deviation of the incoming solar wind from an average direction, aberrated by 4° from the Sun-Earth line. Figure 1 (panel A) shows a histogram of the deviation angle Θ, calculated from three Cartesian components of the solar wind velocity, measured by IMP-8, WIND, and ACE during the period from 1994 to 2002. The histogram is based on 643,568 5-min average data records, and demonstrates that the 5%-, median-, and 95%- values of the deviation angle equal $\approx 0.8°$, $\approx 3.1°$, and $\approx 7.3°$, respectively. The most probable value of the deviation angle equals $\approx 2.5°$ (it is not zero because of the solid angle factor $\sin\Theta$, entering in the probability density per unit deviation angle).

[11] The range of validity of any empirical model critically depends on the data coverage in the geometrical and parametric space. In this work, we derive from observations the response of the current sheet geometry to the dipole tilt and IMF B_y as a function of the solar wind ram pressure P and IMF B_z. A fairly good idea of the data distribution with respect to the above parameters can be gathered from their histograms shown in the panels B, C, and D of Figure 1, based on the same 9-year interval 1994–2002. In each plot, three vertical broken lines correspond to 5%, 50%, and 95% of the total number of 5-min average data records. One can see that 90% of the values of the solar wind control parameters are found within the ranges $0.8 \le P \le 5.6$ nPa, $-6.5 \le B_y \le 6.9$ nT, and $-5.6 \le B_z \le 5.4$ nT, with their median values equal to 2.03 nPa, 0.20 nT, and -0.04 nT, respectively.

2.2. Magnetospheric Magnetic Field Data

[12] As already noted, the magnetospheric observations included in our set covered both the inner low-latitude region (Polar data, $3 \le R \le 9\ R_E$) and the more distant tail (Geotail data, $9 \le R \le 50\ R_E$). In both cases, we started with 1-min resolution data. However, the processing procedures for the Geotail and Polar data were somewhat different, and hence we describe them below in two separate

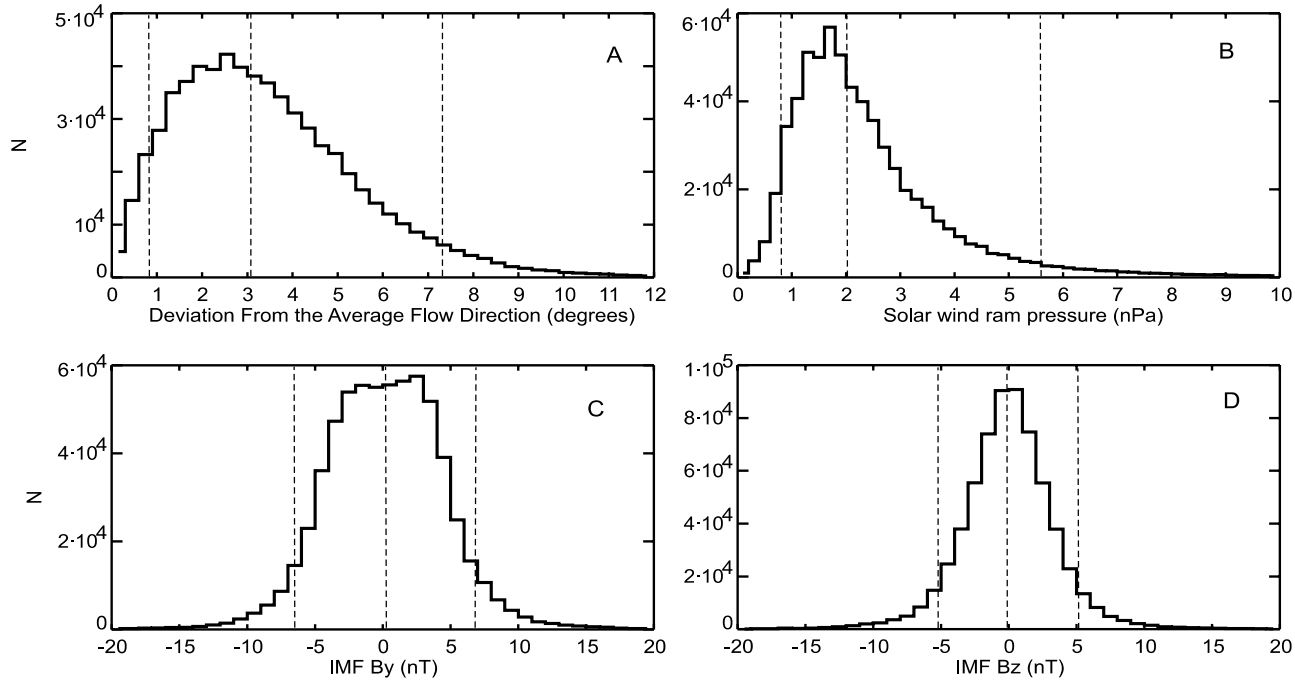

Figure 1

Figure 1. Histograms of the solar wind and interplanetary magnetic field (IMF) parameters, involved in this study. The distributions are based on 643,568 5-minute average data records, taken by IMP 8, Wind, and ACE between 1994 and 2002. Vertical dashed lines in each plot show the 5% (left), median (center), and 95% (right) values. (a) Deviation of the solar wind flow from its average direction, (b) solar wind ram pressure, (c and d) IMF B_Y and B_z, respectively.

sections. Initially we also planned to add GOES-8, -9, and -10 magnetometer data to our data set. However, it was soon realized that because of nearly fixed longitude position of the synchronous spacecraft relatively high above the geomagnetic equatorial plane, they almost never crossed the neutral sheet (more quantitatively, in less than ~0.5% of the total ≈40,000 hours of data) and hence could not provide any significant and reliable information on its position. Note that only nightside data were chosen for this study.

2.2.1. Geotail Data

[13] Magnetic field data of Geotail served as a principal source of information on the shape of the neutral sheet. The original data were first merged into yearly files and corrected for a small B_z offset (see *Tsyganenko* [2002b] for more details). The next step was to filter out solar wind/magnetosheath intervals, using the magnetopause model by *Shue et al.* [1998], driven by concurrent solar wind data (hence this procedure automatically discarded Geotail data without the solar wind/IMF information). After that the 1-min data were averaged over 5-min intervals and converted into the GSM coordinate system.

[14] To further ensure that the Geotail magnetic field data were not contaminated by magnetosheath intervals we took the advantage of the availability of simultaneous LEP plasma instrument data and rejected all intervals with at least one of the following conditions present: (i) the LEP instrument in the solar wind (SW) mode, (ii) $T/N < 5$, where T and N are the proton temperature (keV) and density (cm^{-3}), and (iii) high-speed plasma flows with $|V| >$ 500 km/s. The criterion (ii) was demonstrated earlier [*Tsyganenko and Mukai*, 2003] to effectively discard remaining magnetosheath data records, undetected by the previous filtering based on a magnetopause model.

[15] The final procedure was to convert the Geotail data into the GSW (Geocentric Solar Wind) coordinate system, taking into account the actual direction of the solar wind at Earth's location, corresponding to the time of a magnetospheric field measurement. The GSW coordinate system differs from the standard GSM only in that its X axis is directed anti-parallel to the observed solar wind flow, rather than to Sun's center, which more accurately takes into account the variable aberration effect. To our knowledge, the GSW system was first introduced and described by *Hones et al.* [1986]. A detailed description of the coordinate transformation, converting vectors from GSM to GSW and back, was given by one of us earlier [*Tsyganenko et al.*, 1998] (being then unaware of Hones et al.'s work, we used there the notation GSMSW in place of GSW). Figure 2 shows the distribution of Geotail data used in this work, projected on the GSW equatorial and noon-midnight meridian planes. The total number of Geotail 5-min data records included in the final modeling set was 101,908.

2.2.2. Polar Data

[16] Processing of the Polar MGF experiment data was in principle similar to that of Geotail, but because of the difference in the spatial coverage (much lower apogee) there was no need to use concurrent plasma data at Polar's location. The purpose of including Polar observations was

to properly sample the inner low-latitude magnetosphere; for that reason we selected from the outset only the data taken within a limited sector of solar-magnetic latitude between $-30°$ and $+30°$. We also did not include in the analysis the Polar data taken at $R < 3\ R_E$, as irrelevant to the goal of this study. The data of Polar were also averaged over 5-min intervals; however, because it sampled much lower geocentric distances (where the main geomagnetic field and its gradient are much larger than at the Geotail location), the averaging was actually performed on the external part of the total field, after the internal (IGRF) field was subtracted from the total vector, and then the internal field corresponding to the center of the averaging interval was added back. Figure 3 illustrates the spatial distribution of the Polar data, included in the modeling data set. Except for a different range of $\{X, Y, Z\}$ values, the plot is similar in its format to Figure 2, and the coordinate system used here is also the GSW. The total number of Polar 5-min average data records selected for the final data set was 30,942.

3. Analytical Approximation for the Warped/Twisted Current Sheet

[17] The degree of complexity of any empirical model usually represents a trade-off between our desire to maximize information on the modeled object and natural limitations of the data due to their inaccuracy, limited coverage of the geometrical and parametrical space, and noise effects. The actual instantaneous shape of the tail current sheet can be quite complex and hard to derive, due to the distributed nature of the current with embedded multilayered structures, incessant flapping motion, irregular fluctuations, and wave-like propagating distortions [*Sergeev et al.*, 2003], especially during disturbed periods. In this study we assume a simple single-sheet model of the tail current, replicating only its regular large-scale geometry, and leave out all transient short-lived features. As discussed below, the masking effect of the random fluctuations significantly limits the accuracy of our approximation and its degree of detail, while the limited spatial and parametrical coverage inevitably constrains its validity region.

[18] The average shape of the tail current sheet can be described by specifying the displacement Z_N of the "neutral sheet" (a precise definition of the neutral sheet will be given below) from the GSW equatorial plane, as a function of X and Y. It is convenient to expand Z_N into a sum of three terms, representing the net deformation as a superposition of three effects: (1) a deflection of the neutral sheet from the tilted dipolar equatorial plane in the X-Z plane, (2) a similar tilt-related deflection (warping), but in the Y-Z plane, and (3) a twisting of the neutral sheet around the Sun-Earth line, caused by the B_y component of the IMF. Based on our earlier studies [e.g., *Tsyganenko*, 1998], we adopted the following approximation:

$$Z_N = -X\tan\Psi^* - \left(G_0 + G_1\frac{X}{10}\right)\left(\frac{|Y|}{15}\right)^3 \sin\Psi + S\frac{|X|}{10}\frac{Y}{15}\frac{B_y}{5}, \tag{1}$$

where X, Y, and IMF B_y were normalized by their characteristic values 10 R_E, 15 R_E, and 5 nT, respectively,

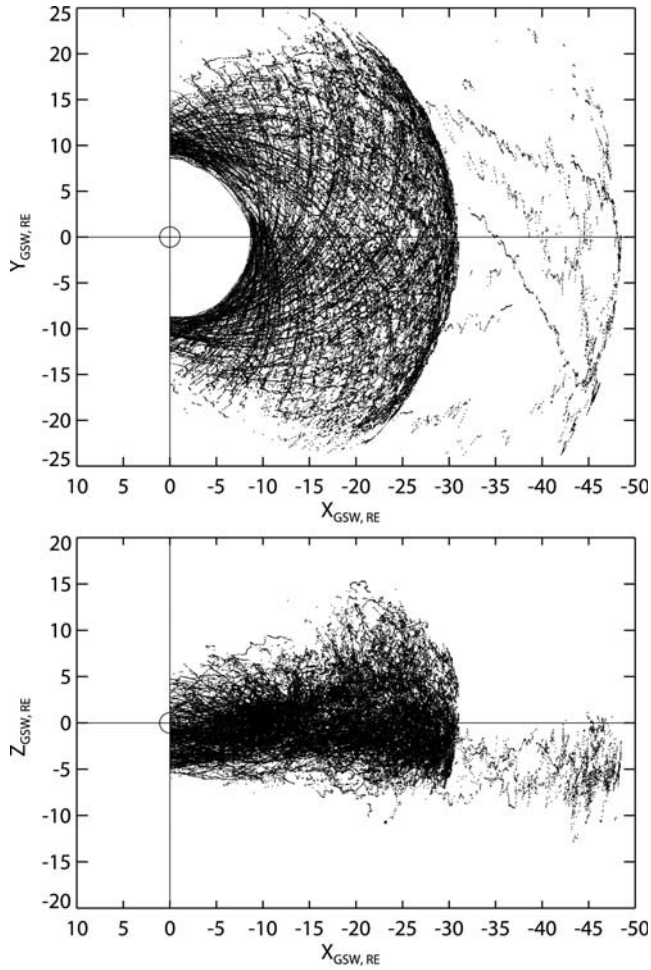

Figure 2. Spatial coverage of the low-latitude magnetosphere by Geotail data used in this study, shown in the GSW equatorial (top) and noon-midnight meridional (bottom) projections. Each dot corresponds to a 5-min average data record, whose total number equals 101,908.

to keep the model coefficients within a convenient range of values.

[19] The "effective" tilt angle Ψ^* in the first term is a function of the actual tilt angle Ψ and of the coordinate X (since our model is limited to the nightside, X is always negative):

$$\sin\Psi^* = \frac{\sin\Psi}{\left[1 + \left(\frac{|X|}{R_H}\right)^{\alpha}\right]^{1/\alpha}} \tag{2}$$

It also includes two parameters: the hinging distance R_H and the power index α. The hinging distance defines the position of the bending on the neutral sheet surface, separating its near-Earth part (closely aligned with the dipole equatorial plane) from the more distant tailward region, where the neutral sheet gradually becomes parallel to the solar wind direction. The value of the parameter α defines the spatial extent of the transition between the two regions (in other words, the sharpness of the hinging area),

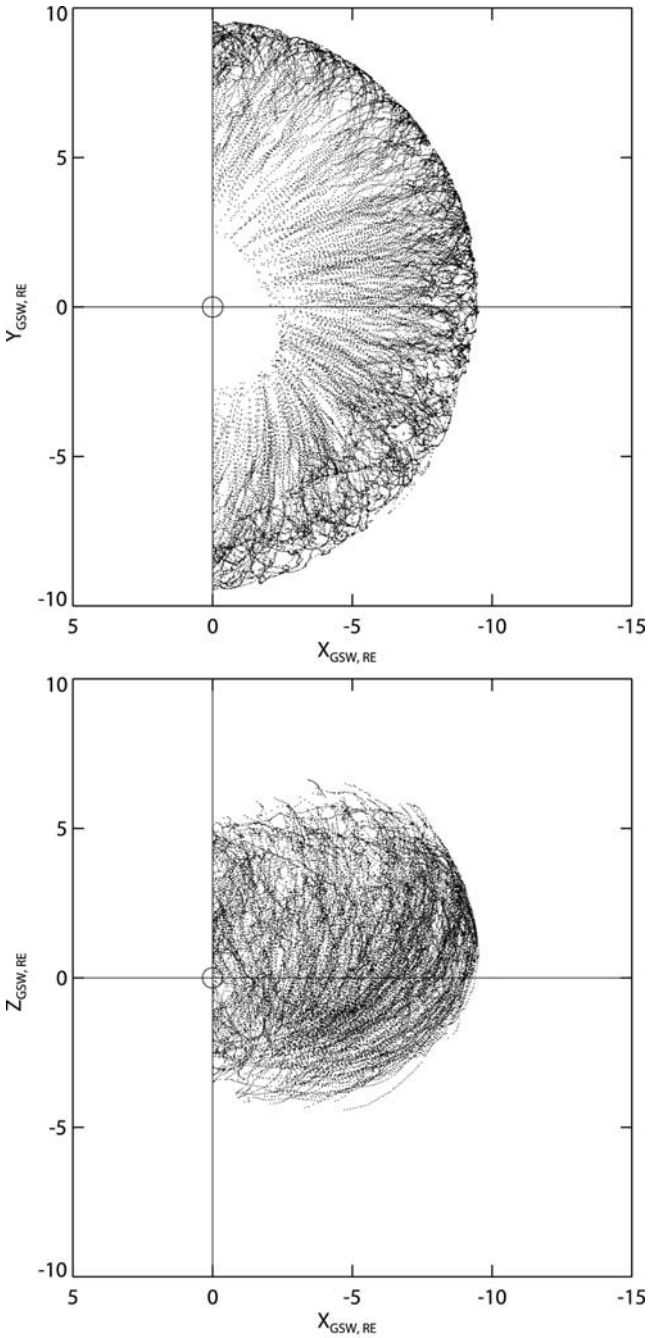

Figure 3. Spatial coverage of the low-latitude inner magnetosphere by Polar data used in this study, shown in the GSW equatorial (top) and noon-midnight meridional (bottom) projections. Each dot corresponds to a 5-min average data record, and their total number equals 30,942.

as illustrated in Figure 4. Larger values of α provide a more abrupt bending of the sheet at the hinging location $X = -R_H$, while smaller values yield a smoother transition. In fact, the present form (2) of sin Ψ^* is a more flexible modification of a previously suggested approximation [*Tsyganenko*, 1998, Section 3, Equations (7)–(14); *Tsyganenko*, 2002a, Equations (7)–(12)], in which a fixed value $\alpha = 3$ was assumed.

[20] In an early version of this study, we also experimented with a more general form of Equation (2), in which an independent power index $1/\beta$ was used in the denominator, instead of $1/\alpha$. Theoretically, that makes it possible to model more general shapes of the current sheet with different types of variation of Z_N with the tailward distance X. In that approximation, for $\alpha < \beta$ the neutral sheet monotonically departs from the GSW equatorial plane with growing tailward distance, in the case $\alpha = \beta$ it asymptotically becomes parallel to the Sun-Earth line, and for $\alpha > \beta$ the distance between the neutral sheet and the equatorial plane is a non-monotonic function of X, so that at a sufficiently large $|X|$ the neutral sheet gradually returns back to the equatorial plane. However, the derivation of unique best fit values of both α and β was found to be severely hindered by a generally shallow and uneven shape of the surface of the target function in the multiparameter space, as discussed in more detail in the next sections. For that reason, we eventually chose a simpler form (2) with $\beta \equiv \alpha$.

[21] The magnitude of the transverse warping as defined by the second term in (1) is controlled by the coefficient $G = G_0 + G_1 (X/10)$, the sine of the dipole tilt angle Ψ, and the factor $(Y/15)^3$, defining the cross-tail profile of the current sheet. By testing many possible approximations, we found that, within the limited range of the tailward distance $-50\ R_E \leq X \leq 0$ covered by the data, there was little sense in using any other function than the simplest linear variation with X, employed in (1). Likewise, as we explored more sophisticated cross-tail shapes of the current sheet, we found that none of them provided a tangible improvement over the simple function $F(Y) = (|Y|/15)_\gamma$. Best-fit values of the power index γ, derived from many subsets of data, in all cases were found to be close to $\gamma = 3$, and that value was adopted for the final approximation (1).

[22] The third term in (1), unlike the second one, is an odd (linear) function of Y and, for that reason, yields a twisting of the model neutral sheet around the tail axis. We also assumed that the twisting effect is proportional to the IMF B_y and linearly increases down the tail with growing $|X|$. The last assumption appears reasonable only in the near-tail region, and was made here solely because of a limited spread of our data along the tail (within $|X| \leq 50\ R_E$). In the asymptotic limit $|X| \rightarrow \infty$ it yields the twist angles equal to $\pm 90°$ regardless of the actual IMF clock angle, which is obviously incorrect. In actu-

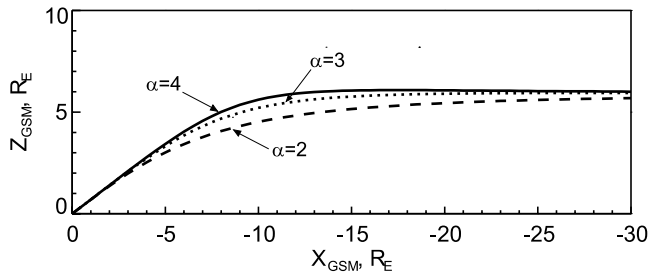

Figure 4. Illustrating the model approximation (1)–(2) for the global shape of the neutral sheet. The plot shows midnight meridian sections of the deformed neutral sheet for the maximal tilt angle of the Earth's dipole ($\Psi = 35°$) and three different values of the parameter α.

ality, the asymptotic orientation of the current sheet should depend on the polarities and relative magnitudes of both B_y and B_z components of the IMF, as was demonstrated by *Maezawa and Hori* [1998] using deep-tail Geotail observations.

4. Parameterization and Fitting to the Data

[23] The approximation (1)–(2) for the global shape of the neutral sheet includes 5 parameters (R_H, α, G_0, G_1, and S) and uniquely defines Z_N as a function of X and Y, for any values of the dipole tilt Ψ and IMF B_y. The fitting method was based on minimizing the number of mismatches between the observed orientation of the magnetic field and that predicted by the model. This approach was used in an early work by one of us [*Fairfield*, 1980], to derive the shape of the midtail neutral sheet at $X < -20\ R_E$. In contrast to that effort, the present study addresses the global shape of the tail current sheet, including not only the middle tail with mostly sunward/antisunward **B** in the lobes, but also the near-Earth dawn and dusk sectors, where the magnetic field vector has a significant component in the Y-direction and the current sheet warps in two dimensions. Because of that, we needed to accurately define the neutral sheet and to devise a convenient criterion to determine the position of the spacecraft with respect to that sheet.

[24] We define the neutral sheet as a warped surface, across which the tangential component of the **B** vector (calculated with respect to that surface) reverses its direction. Since the magnetotail current is flowing mostly in the azimuthal direction, the principal part of the **B** vector that reverses its orientation on crossing the sheet lies in the solar magnetic (SM) meridian plane. Based on that, we defined the neutral sheet as a surface at which

$$\mathbf{B} \cdot \left(\mathbf{n} \times \mathbf{e}_\phi\right) = 0, \tag{3}$$

where $\mathbf{n}$ is a unit normal vector to the surface and $\mathbf{e}_\phi$ is the unit vector in the direction of increasing SM longitude. The lefthand side of (3) approximately (to within a normalization factor on the order of unity) equals the magnitude of the field component lying in the plane of the SM meridian and tangential to the neutral sheet. It can be calculated from the observed field vector and the neutral sheet model (1)–(2), and we use its sign as an indicator of the spacecraft position with respect to the warped neutral sheet. Even though we do not know the distance of the observation point from the neutral sheet, we still can project it on the sheet along the Z axis (since it does not depend on Z) and calculate there the direction of the normal vector $\mathbf{n}$ as

$$\mathbf{n} = \frac{\nabla\Phi}{|\nabla\Phi|}, \tag{4}$$

where the scalar function $\Phi = Z - Z_N$ is defined by the neutral sheet model (1)–(2), and then determine the sign of the lefthand side of (3). Positive (negative) values of $\mathbf{B} \cdot (\mathbf{n} \times \mathbf{e}_\phi)$ indicate that the observation point is located northward (southward) from the model neutral sheet. If the sign of $\mathbf{B} \cdot (\mathbf{n} \times \mathbf{e}_\phi)$ is the same as of $\Phi = Z - Z_N$, then the model prediction matches the observation, otherwise we have a mismatch. The ratio Q of the number of mismatches to the total number of data records in the entire data set was used as a target function of the neutral sheet model. By making a search in the model parameter space, we minimized Q and obtained a best-fit representation of the neutral sheet. Note, however, that our method did not use least squares and hence there was no straightforward way to linearize the problem. Another complication resulted from the discontinuous nature of our target function, defined to be proportional to the integer number of mismatches. That prevented us from using nonlinear search algorithms based on its derivatives with respect to the model parameters (which in our case are zero almost everywhere). Since we could not use a standard inversion technique, the model parameters were derived in two steps. We first calculated values of the target function in the nodes of a mesh, covering a wide region in the 5-dimensional parametrical space, and thus approximately straddled the minimum of the target function. After that, a refined search was made using a simplex algorithm [*Press et al.*, 1992].

[25] First of all, it is interesting to estimate the overall significance of the deformation effect in terms of our target function, as well as the relative importance of three types of the deformation represented by three terms in the righthand side of (1). A natural way to do that is to calculate first the percentage of mismatches, assuming no deformation at all (that is, using a flat current sheet lying in the GSW equatorial plane), and then include each of the three terms, one at a time, fitting the increasingly complex model to the data. The corresponding values of the target function will provide a measure of the model improvement due to its increased flexibility and hence an estimate of the significance of each term. Assuming no deformation at all yielded $Q = 0.240$, in other words, in about a quarter of cases the observed sign of $\mathbf{B} \cdot (\mathbf{n} \times \mathbf{e}_\phi)$ was inconsistent with that expected from the model. Taking into account the bending of the sheet in the X-Z plane (by including only the first term in (1)) more than doubled the accuracy of the model, so that the target function dropped to $Q = 0.109$. Inclusion of the warping effect, replicated by the second term in (1), resulted in its further decrease down to $Q = 0.084$, and taking into account the twisting (third term) yielded $Q = 0.076$. The above result yields a quantitative idea of the hierarchy of the three types of the current sheet deformation represented by (1). It is also interesting to compare the numbers of matches and mismatches for individual spacecraft. In the most accurate approximation with all three terms, the Geotail data yielded 4801 mismatches with $\mathbf{B} \cdot (\mathbf{n} \times \mathbf{e}_\phi) > 0$ but $Z - Z_N < 0$, and 4832 mismatches with the opposite inequality signs, out of the total of 101,908 data records. The corresponding numbers for Polar were significantly lower: 154 and 307 mismatches, respectively, out of the total of 30,942 data records. This is a natural consequence of a larger range of the GSW latitude covered by Polar, in comparison with Geotail, and a more ordered geometry of the current sheet in the inner magnetosphere.

[26] In this study we aimed to derive not only an average tilt-and IMF B_y-dependent shape of the neutral sheet, but also its variation with the solar wind ram pressure P_{dyn} and IMF B_z component. A straightforward way for doing that is to represent the above 5 parameters as empirical functions

Table 1. Parameters of the Model Neutral Sheet From Subsets of Data for 5 Bins of the Solar Wind Pressure

P (nPa)	[0, 1]	[1, 2]	[2, 3]	[3, 4]	>4
N	12135	40912	23147	8014	5214
$\langle P \rangle$	0.76	1.5	2.4	3.4	5.6
Q	0.054	0.069	0.078	0.085	0.084
R_H	16.7	11.3	8.66	8.50	8.81
α	1.28	2.10	2.79	2.26	2.87
G_0	9.37	14.4	16.3	16.9	26.3
G_1	1.43	2.81	3.93	3.38	7.31
S	0.51	0.87	0.56	0.52	0.61

of P_{dyn} and IMF B_z and then fit the model to the entire body of the data. However, as we did not have much apriori knowledge on the actual response of the model parameters to the solar wind and IMF state, our approach here was twofold. First, a preliminary calculation was made of the model parameter dependence on the solar wind/IMF characteristics, by binning all the data into several intervals of P_{dyn} and IMF B_z and then deriving best fit values of the 5 model parameters for each bin. The second step was to devise a "global" form of the model, providing suitable analytical approximations for the 5 parameters, based on the observed trends of their bin-to-bin variation with P_{dyn} and/or IMF B_z. The initial values of the model parameters for the global fitting runs were also specified on the basis of the binning results, and the fitting procedure was performed using the entire body of the data, as described below in more detail.

5. Results

[27] Tables 1 and 2 present the results of the preliminary study where the 5 model parameters were calculated for 5 bins of the solar wind ram pressure P and for 7 bins of the IMF B_z (GSM) component. When binning the data with respect to each of the two parameters, it was required that the other parameter was confined within a relatively limited range, to more clearly separate their effects on the shape of the current sheet. Thus the data binned into the 5 intervals of P included only those observations, for which $-2 \le B_z \le 3$ nT. Likewise, the binning with respect to the IMF B_z was made under an additional requirement $1 \le P \le 3$ nPa.

[28] The following trends become apparent from inspecting the parameter values. (1) The hinging distance R_H significantly decreases with growing P, especially between the first two bins of the pressure. It also appears to generally decrease as the IMF changes from southward to northward. (2) The parameter α increases with growing P, with some irregularity at the high end of the range. It also shows a similar behavior with respect to the IMF B_z: a steady increase with B_z varying from large negative values toward zero, but a more irregular variation for $B_z > 0$. (3) The transverse warping amplitude, G_0, increases with pressure and so does its tailward variation rate G_1. Note that the coefficient G_1 is positive, which means a significant reduction of the warping with growing tailward distance, in agreement with our earlier finding [*Tsyganenko et al.*, 1998]. However, no ordered dependence on the IMF B_z was found for these two coefficients. (4) The twisting amplitude does not show any regular dependence on the solar wind pressure, but it significantly increases with growing positive IMF B_z, especially between the last two bins.

[29] Taking into account all these facts, we tried several approximations for the five model parameters as functions of P and B_z, with different degrees of complexity. The following form was eventually adopted as a final version:

$$R_H = \left(R_{H0} + R_{H1}\frac{B_z}{B_{z0}}\right)\left(\frac{P}{P_0}\right)^{\chi} \quad G_0 = G_{00} + G_{01}\frac{P}{P_0}$$

$$G_1 = G_{10} + G_{11}\frac{P}{P_0} \quad \alpha = \alpha_0 + \alpha_1\frac{B_z}{B_{z0}} \quad S = S_0 + S_1 \exp\left(\frac{B_z}{B_{z0}}\right), \tag{5}$$

where P and B_z were also normalized by their characteristic values, $P_0 = 2$ nPa and $B_{z0} = 5$ nT. This choice was based on comparing relative improvements of the global target function Q obtained in many trial runs, and the requirement that the analytical model remain as simple as possible. For example, initially the equation for α also included a linear dependence on the pressure, but, somewhat surprisingly, taking out that term virtually did not affect the target function Q.

[30] Since the approximation (5) uses a linear dependence of R_H, G, and α on P and B_z, and an exponent of B_z/B_{z0} in the twisting coefficient S, we set an additional restriction on the data by requiring that $0 < P \le 6$ nPa and $|B_z| \le 10$ nT. By doing so, we eliminated a relatively small group of data records corresponding to unusual solar wind and/or IMF conditions, in order to avoid extrapolation of (5) beyond the commonly observed range of P and B_z (which could otherwise result in biased values of the model parameters). The total number of records in the final data set used in the global fitting of the model parameters was 132,850 (against 139,690 in the original unabridged set).

[31] Equations (1)–(2) and (5) provide a complete formulation of the neutral sheet model, and Table 3 summarizes the results of its fitting to the entire set of Geotail and Polar data, along with the values of uncertainties. The uncertainties were estimated using the bootstrap method, based on a number of resampled subsets with the same number of data records as in the original data set, but with a fraction of the data being randomly replaced by duplicated original records. In this particular realization of the bootstrap approach, we created 25 random subsets and calculated the uncertainties of individual parameters based on the range of the dispersion of their 25 best-fit values. The overall value of the target function for the global approximation (1)–(2) and (5) equals

Table 2. Parameters of the Model Neutral Sheet From Subsets of Data for Seven Bins of the IMF B_z

B_z (nT)	< −4	[−4, −2]	[−2, −.5]	[−.5, .5]	[.5, 2]	[2, 4]	>4
N	7222	14764	20792	15890	19319	12863	5125
$\langle B_z \rangle$	−6.2	−2.8	−1.2	0.05	1.3	2.9	5.8
Q	0.072	0.064	0.076	0.075	0.070	0.058	0.063
R_H	13.1	11.7	9.1	8.6	9.8	9.0	8.3
α	1.50	1.79	2.62	3.78	2.04	2.41	2.17
G_0	13.4	14.7	16.7	13.5	16.0	13.6	12.1
G_1	2.54	3.54	4.84	2.60	3.16	2.46	2.17
S	0.57	0.58	0.67	0.74	0.84	0.83	1.22

$Q = 0.070$. Comparing this value with $Q = 0.076$, obtained using the same model (1)–(2) but without any dependence on the solar wind pressure and IMF B_z (previous section), one sees that including the interplanetary parameters improves the target function by ≈8%.

[32] The average shape of the neutral sheet and its dependence on the solar wind and IMF as derived from the model, is illustrated in Figures 5–7, each showing a family of cross-sections of the sheet by equidistant planes $X = -5, -10, -15, \ldots, -50\ R_E$. The effect of the solar wind pressure P on the tilt-related warping of the neutral sheet can be clearly seen in Figure 5, comparing the shapes for P = 1 nPa (top) and P = 6 nPa. These values approximately correspond to the 5% and 95% pressure levels in Figure 1, roughly delineating the limits of the model's validity with respect to P. Both panels correspond to the maximal positive value of the tilt angle $\Psi = 35°$ and IMF $B_y = 0$. As can be seen from the plots, the decrease of the hinging distance with growing solar wind pressure results in a lesser amplitude of the north-south motion of the neutral sheet near the midnight meridian. At the same time, the increase of the warping amplitude G with growing P results in a larger amplitude of the oppositely directed shift of the neutral sheet at the flanks of the near-Earth tail. At larger tailward distances, owing to the linear decrease of G, the neutral sheet gradually flattens, so that the reversal from northward to southward location occurs at progressively larger distances from the midnight meridian, than in the near tail.

[33] Figure 6, similar in format to Figure 5, demonstrates the effect of the IMF B_z by comparing the shapes of the warped model neutral sheet for the same values of $\Psi = 35°$, P = 2 nPa, and IMF B_y, but for two opposite polarities of IMF B_z, equal to −5 nT (top) and +5 nT (bottom). As clearly seen, negative IMF B_z results in a more gradual bending of the neutral sheet in the near tail, and hence significantly larger amplitude of the north-south excursion of the sheet in the midtail. This can be viewed as a consequence of a larger magnetic flux in the tail lobes during periods of southward IMF, and hence a less flexible tail, more rigidly tied to the tilted dipole. As demonstrated below, this interpretation is consistent with a similar effect of the IMF B_z on the IMF B_y-related twisting.

[34] Figure 7 illustrates the counter-clockwise twisting of the sheet around the GSW X-axis. It displays a family of neutral sheet cross-sections for untilted dipole, average P = 2 nPa, but non-zero IMF B_y = 7 nT (also, roughly at the 95% level of its occurrence frequency, according to Figure 1). As

Table 3. Global Parameters of the Model Neutral Sheet, Entering in Equations (1)–(2) and (5)

Parameter	Value	Uncertainty
R_{H0}	10.28	±0.70
R_{H1}	−1.50	±0.15
χ	−0.228	±0.020
α_0	1.99	±0.013
α_1	0.256	±0.023
G_{00}	9.38	±0.70
G_{01}	4.83	±0.40
G_{10}	1.79	±0.10
G_{11}	0.955	±0.06
S_0	0.356	±0.050
S_1	0.285	±0.025

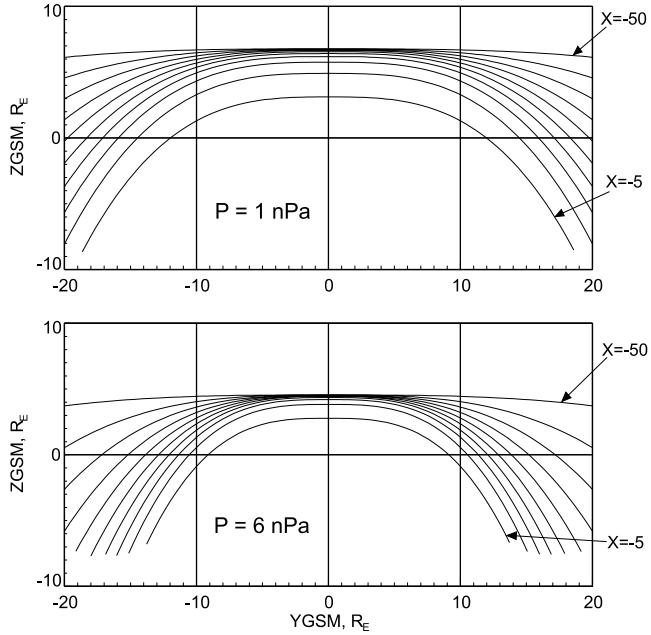

Figure 5. Comparing the shapes of the warped neutral sheet for average (top) and large (bottom) values of the dynamic pressure of the solar wind. Families of cross sections in each panel correspond to equidistant planes, crossing the Sun-Earth line at $X = -5, -10, -15, \ldots, -50\ R_E$. The endpoints of the near-tail contours that do not reach the plot frames correspond to the position of the model magnetopause of *Shue et al.* [1998].

in the previous figure, top and bottom panels corresponds to IMF $B_z = -5$ nT and +5 nT, respectively. A significantly larger degree of twisting in the latter case fully agrees with earlier findings [*Owen et al.*, 1995; *Maezawa et al.*, 1997],

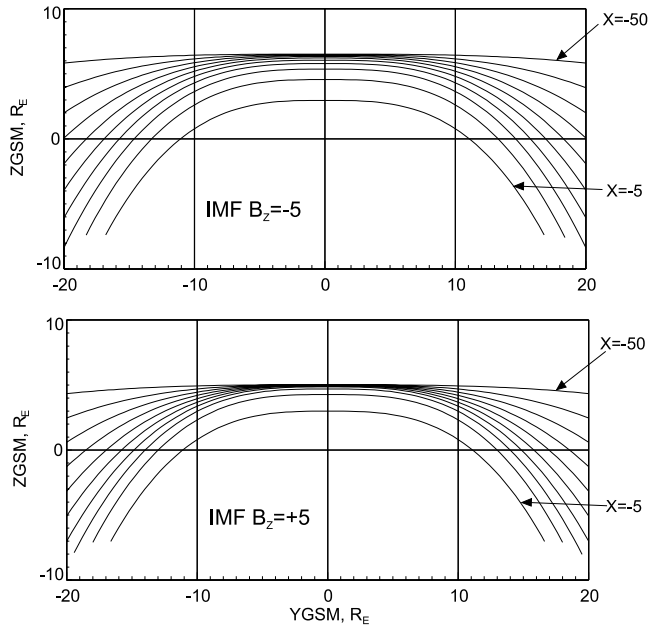

Figure 6. Same as in Figure 5, but for two opposite polarities of the IMF B_z: (top) $B_z = -5$ nT and (bottom) B_z = +5 nT.

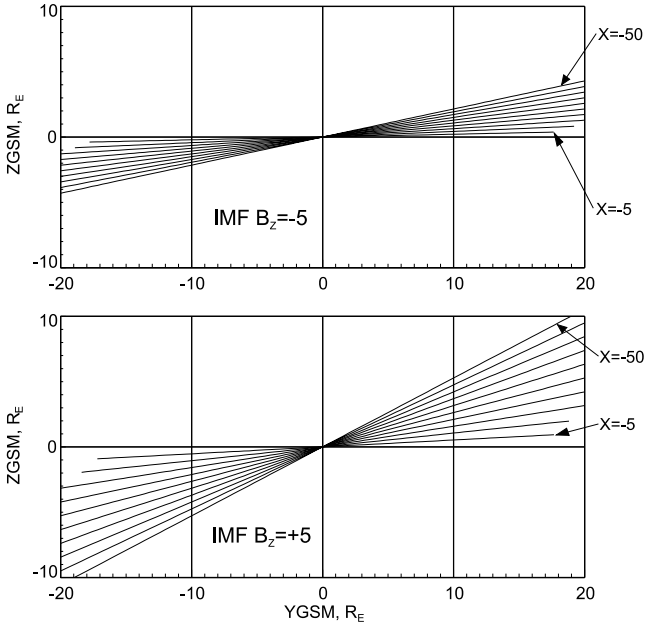

Figure 7. Illustrating the effect of the IMF B_y-related twisting of the neutral sheet and its dependence on the IMF B_z, using the same format as in Figures 5 and 6. In this example IMF B_y = 7 nT. Note a much larger twisting in the case of northward IMF B_z.

and confirms much larger susceptibility of the tail to external stresses, induced by the IMF during periods with northward polarity.

6. Discussion and Conclusions

[35] It is interesting to compare the results of this study with our earlier calculations [*Tsyganenko et al.*, 1998], in which we used a smaller set of Geotail data (binned into 7 intervals of X) and a completely different fitting method. Figure 8 compares the shape of the warped neutral sheet cross sections for $\Psi = 35^\circ$ at 6 different tailward distances, corresponding to the centers of 6 first bins of X_{GSW} in that work. Solid and dotted lines correspond, respectively, to the present (Equations (1), (2), and (5)) and the old model. The values of the solar wind parameters in the new model were assumed equal to their average values: P = 2 nPa, and IMF $B_y = B_z = 0$. The agreement between the two approximations is fairly good in the near and middle tail ($X_{GSW} \geq -35\ R_E$), where the deviation between model surfaces is typically within 1.0–1.5 R_E. At larger tailward distances the new model predicts systematically larger deflection of the neutral sheet from the GSW equatorial plane, than did the earlier calculation, especially near the dawn and dusk sides of the tail, where the discrepancies rise to $\sim$5 R_E.

[36] Figure 9, similar in its format to Figure 8, compares the twisting effect of the IMF B_y, as reproduced by the new and old approximations. Here the dipole tilt angle was

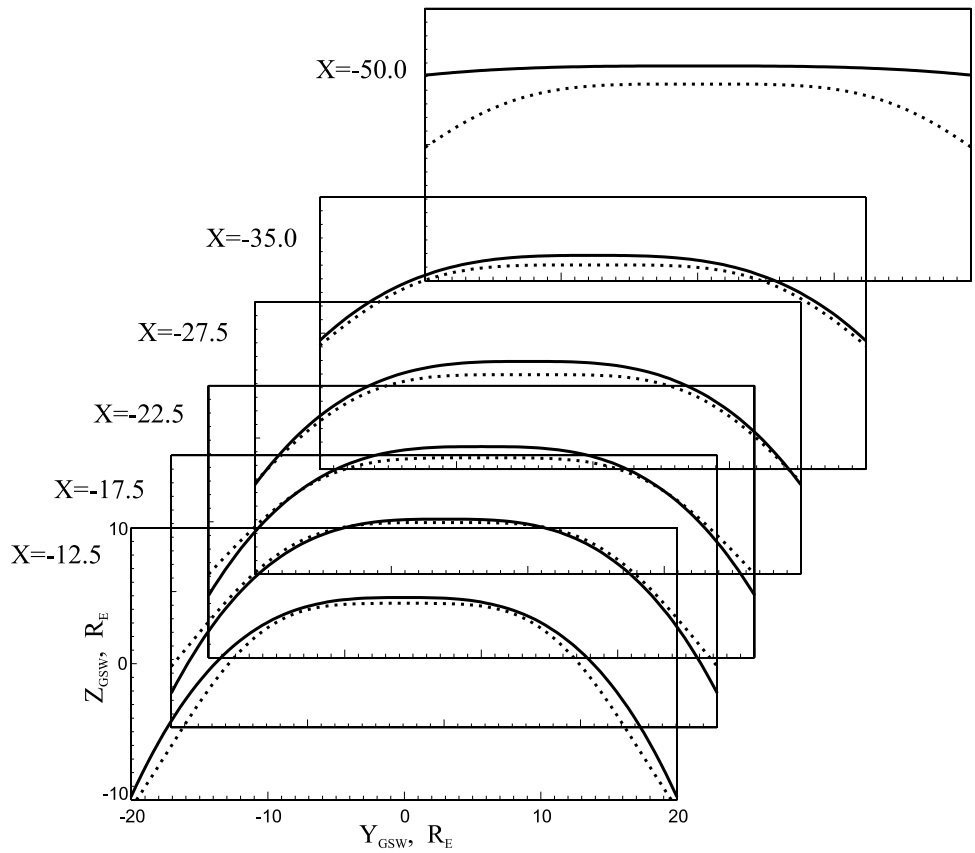

Figure 8. Illustrating the 3D shape of the model warped neutral sheet for $\Psi = 35^\circ$ (solid contours) in comparison with our earlier result (dotted lines).

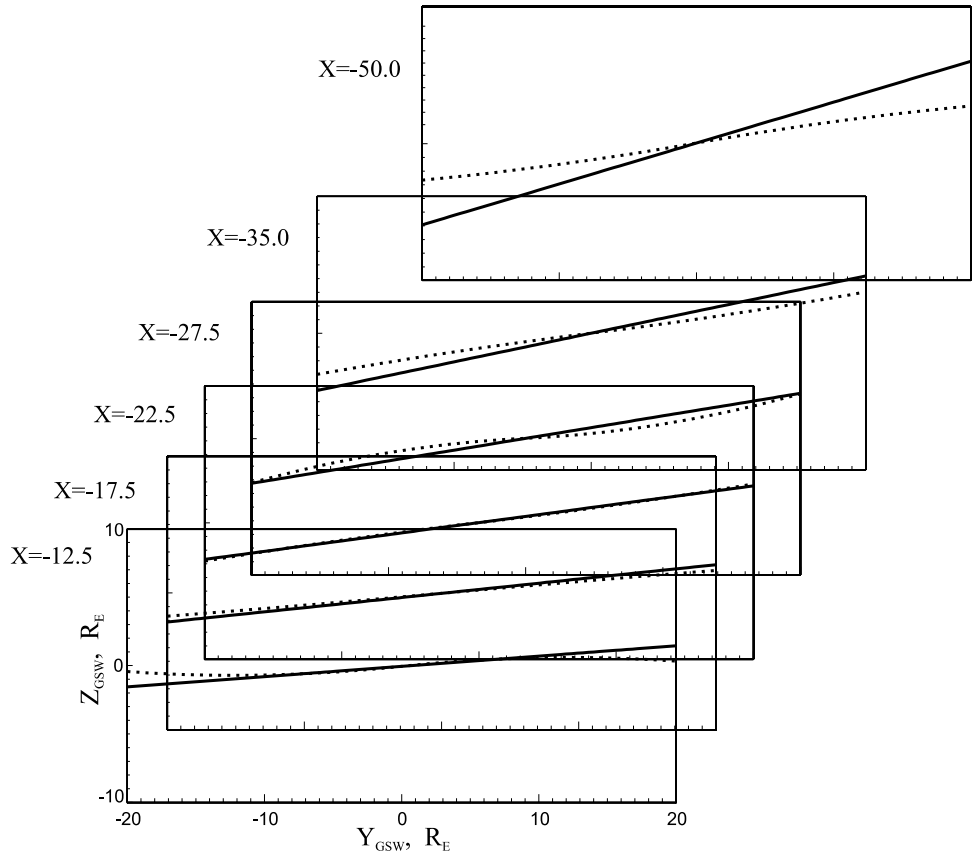

Figure 9. Same as in Figure 8, but for the twisting effect by the IMF B_y = 7 nT, with zero geodipole tilt.

assumed zero, P = 2 nPa, IMF B_y = 7 nT, and B_z = 0. In general, the new model predicts larger twisting angles at all distances. Note that the old approximation for Z_N included a cubic term with respect to Y, introduced in order to take into account a possible S-shaped deformation of the current sheet. As can be seen from the plot, such a nonlinear distortion was significant only in the nearest bin of X, but it remained unclear if that was a real effect or just a

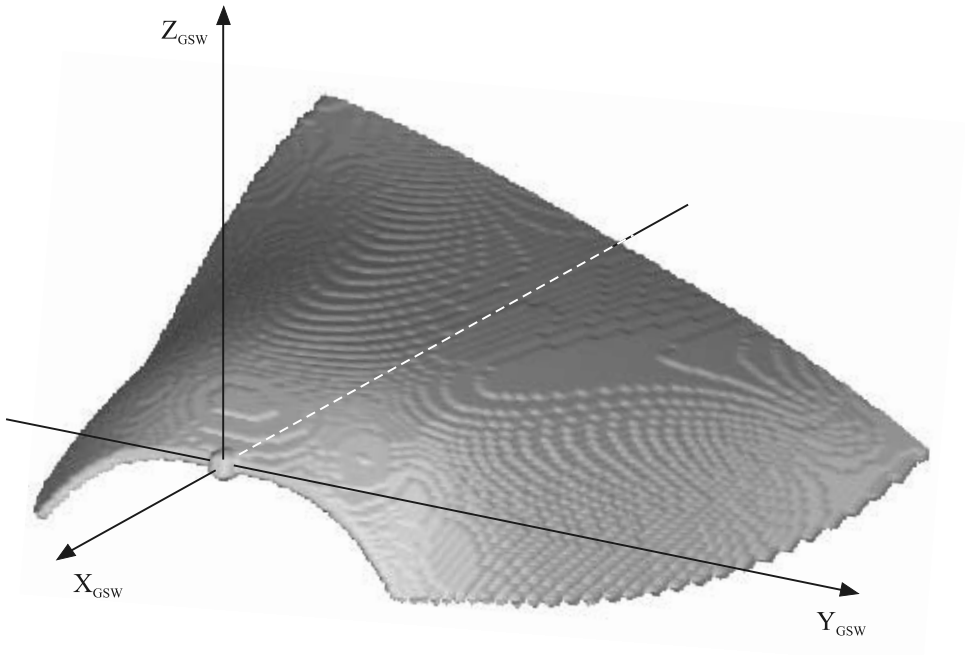

Figure 10. A three-dimensional view of the warped and twisted tail neutral sheet, obtained for $\Psi = 35°$, IMF $B_y = -7$ nT, P = 2 nPa, and IMF B_z = 0.

modeling artifact. In this work, we restricted the model to only a linear dependence of Z_N on Y, which ignored the possibility of the S-shaped twisting of the neutral sheet by retaining only the principal linear term. The closest agreement between the models was found for $X = -22.5\ R_E$ (3rd panel from bottom of the plot), where the solid and dotted lines almost coincide. At larger tailward distances the discrepancy steadily increases and becomes quite significant at $X = -50\ R_E$, where the new model predicts the rotation about twice as large as in the old one.

[37] To give readers a clearer sense of the general range of the neutral sheet deformation, we reproduce in Figure 10 a 3D view of the model surface, calculated from (1)–(2) and (5) for $\Psi = 35°$ and IMF $B_y = -7$ nT. The solar wind pressure and IMF B_z were assumed equal to their average values $P = 2$ nPa and $B_z = 0$. On the nightside the surface extends to $X = -50\ R_E$, which roughly corresponds to the tailward validity limit of the model. This estimate is based on the overall spatial extent of the data used in this study (Figure 2); however, one should keep in mind that the data coverage in the interval $-50 \le X \le -30\ R_E$ is much poorer than at closer distances, so that the model's accuracy in that region relies on the validity of the linear approximation adopted in (1).

[38] In summary, we developed a new analytical approximation for the global shape of the tail neutral sheet, parameterized by the tilt of the Earth's dipole, solar wind pressure, and the transverse components of the IMF, B_y and B_z. Numerical values of the model parameters were found by minimizing the total number of mismatches between the predicted and observed orientation of the magnetic field, based on 9 years of Geotail and 3 years of Polar data, taken in the proximity of the plasma sheet. Variations of the solar wind pressure P change the shape of the deformed current sheet in such a way that an increase of P results in a decrease of the magnetotail "hinging distance" R_H, but increases the magnitude of its transverse warping. The IMF B_z component affects the magnitude of the seasonal/diurnal motion of the current sheet in the north-south direction, and it also controls the degree of the IMF B_y-related twisting, which becomes much larger during the periods with northward IMF B_z, in agreement with earlier published studies.

[39] **Acknowledgments.** It is a pleasure to acknowledge the teams and PIs of all experiments, whose data were used in this study. Geotail MGF data were provided by the PIs, S. Kokubun (STEL) and T. Nagai (Tokyo Institute of Technology, Japan). The data of Polar MGF experiment were made available by the UCLA team led by the PI C. T. Russell. Interplanetary medium data of Wind (K. Ogilvie and R. Lepping, NASA GSFC), IMP 8 (A. Lazarus, MIT, and R. Lepping, NASA GSFC), and ACE (D. McComas, LANL, and N. Ness, Bartol Research Institute) were obtained from NSSDC via CDAWEB online facility. This work was supported by NSF grants ATM-0296212 and by NASA's LWS grant NAG5-12185.

[40] Lou-Chuang Lee thanks Kiyoshi Maezawa and Christopher J. Owen for their assistance in evaluating this paper.

References

Dandouras, J. (1988), On the average shape and position of the geomagnetic neutral sheet and its influence on plasma sheet ststistical studies, *J. Geophys. Res.*, *93*, 7345.

Efron, B., and R. Tibshirani (1993), *An introduction to the bootstrap*, Chapman and Hall, New York.

Fairfield, D. H. (1980), A statistical determination of the shape and position of the geomagnetic neutral sheet, *J. Geophys. Res.*, *85*, 775.

Gosling, J. T., D. J. McComas, M. F. Thomsen, S. J. Bame, and C. T. Russell (1986), The warped neutral sheet and plasma sheet in the near-Earth geomagnetic tail, *J. Geophys. Res.*, *91*, 7093.

Hones, E. W., R. D. Zwickl, T. A. Fritz, and S. J. Bame (1986), Structural and dynamical aspects of the distant magnetotail determined from ISEE-3 plasma measurements, *Planet. Space Sci.*, *34*, 889.

Lopez, R. E. (1990), The position of the magnetotail neutral sheet in the near-Earth region, *Geophys. Res. Lett.*, *17*, 1617.

Maezawa, K., and T. Hori (1998), The distant magnetotail: Its structure, IMF dependence, and thermal properties, in *New Perspectives on the Earth's Magnetotail*, *Geophys. Monogr. Ser.*, vol. 105, edited by A. Nishida, D. N. Baker, and S. W. H. Cowley, pp. 1–19, AGU, Washington, D. C.

Maezawa, K., T. Hori, T. Mukai, Y. Saito, T. Yamamoto, S. Kokubun, and A. Nishida (1997), Structure of the distant magnetotail and its dependence on the IMF B_y component: Geotail observations, *Adv. Space Res.*, *20*, 949.

Nakai, H., Y. Kamide, and C. T. Russell (1997), Statistical nature of the magnetotail current in the near-Earth region, *J. Geophys. Res.*, *102*(A5), 9573.

Owen, C. J., J. A. Slavin, I. G. Richardson, N. Murphy, and R. J. Hynds (1995), Average motion, structure and orientation of the distant magnetotail determined from remote sensing of the edge of the plasma sheet boundary layer with $E > 35$ keV ions, *J. Geophys. Res.*, *100*, 185.

Press, W. H., S. A. Teukolsky, W. T. Vetterling, and B. P. Flannery (1992), *Numerical Recipes*, 2nd ed., Cambridge Univ. Press, New York.

Richardson, J. D., and K. I. Paularena (2001), Plasma and magnetic field correlations in the solar wind, *J. Geophys. Res.*, *106*, 239.

Russell, C. T. (1972), The configuration of the magnetosphere, in *Critical Problems of Magnetospheric Physics*, edited by E. R. Dyer, pp. 1–16, IUCSTP Sec., Natl. Acad. of Sci., Washington, D. C.

Russell, C. T., and K. I. Brody (1967), Some remarks on the position and shape of the neutral sheet, *J. Geophys. Res.*, *72*, 6104.

Sergeev, V., et al. (2003), Current sheet flapping motion and structure observed by Cluster, *Geophys. Res. Lett.*, *30*(6), 1327, doi:10.1029/2002GL016500.

Shue, J.-H., et al. (1998), Magnetopause location under extreme solar wind conditions, *J. Geophys. Res.*, *103*, 17,691.

Sibeck, D. G., G. L. Siscoe, J. A. Slavin, E. J. Smith, B. T. Tsurutani, and R. P. Lepping (1985), The distant magnetotail's response to a strong interplanetary magnetic field B_y: Twisting, flattening, and field line bending, *J. Geophys. Res.*, *90*, 4011.

Tsyganenko, N. A. (1998), Modeling of twisted/warped magnetospheric configurations using the general deformation method, *J. Geophys. Res.*, *103*, 23,551.

Tsyganenko, N. A. (2002a), A model of the near magnetosphere with a dawn-dusk asymmetry: 1. Mathematical structure, *J. Geophys. Res.*, *107*(A8), 1179, doi:10.1029/2001JA000219.

Tsyganenko, N. A. (2002b), A model of the near magnetosphere with a dawn-dusk asymmetry: 2. Parameterization and fitting to observations, *J. Geophys. Res.*, *107*(A8), 1176, doi:10.1029/2001JA000220.

Tsyganenko, N. A., and T. Mukai (2003), Tail plasma sheet models derived from Geotail particle data, *J. Geophys. Res.*, *108*(A3), 1136, doi:10.1029/2002JA009707.

Tsyganenko, N. A., S. B. P. Karlsson, S. Kokubun, T. Yamamoto, A. J. Lazarus, K. W. Ogilvie, and C. T. Russell (1998), Global configuration of the magnetotail current sheet as derived from Geotail, Wind, IMP 8, and ISEE 1/2 data, *J. Geophys. Res.*, *103*, 6827.

Tsyganenko, N. A., G. Le, C. T. Russell, and T. Iyemori (1999), A study of the inner magnetosphere based on data of Polar, *J. Geophys. Res.*, *104*, 10,275.

D. H. Fairfield, Laboratory for Extraterrestrial Physics, NASA Goddard Space Flight Center, Greenbelt, MD 20771, USA. (donald.h.fairfield@nasa.gov)

N. A. Tsyganenko, Universities Space Research Association and Laboratory for Extraterrestrial Physics, Code 695, NASA Goddard Space Flight Center, Greenbelt, MD 20771, USA. (nikolai.tsyganenko@gsfc.nasa.gov)